CrossMark

JFM PAPERS

Inverse cascade suppression and shear-layer formation in magnetohydrodynamic turbulence subject to a guide field and misaligned rotation

Santiago J. Benavides[1,†], **Keaton J. Burns**[2,3], **Basile Gallet**[4], **James Y-K. Cho**[3] **and Glenn R. Flierl**[1]

[1]Department of Earth, Atmospheric, and Planetary Sciences, Massachusetts Institute of Technology, Cambridge, MA 02139 USA

[2]Department of Mathematics, Massachusetts Institute of Technology, Cambridge, MA 02139 USA

[3]Center for Computational Astrophysics, Flatiron Institute, New York, NY 10010 USA

[4]Université Paris-Saclay, CNRS, CEA, Service de Physique de l'Etat Condensé, 91191 Gif-sur-Yvette, France

Astrophysical flows are often subject to both rotation and large-scale background magnetic fields. Individually, each is known to two-dimensionalize the flow in the perpendicular plane. In realistic settings, both of these effects are simultaneously present and, importantly, need not be aligned. In this work, we numerically investigate three-dimensional forced magnetohydrodynamic turbulence subject to the competing effects of global rotation and a perpendicular background magnetic field. We focus on the case of a strong background field and find that increasing the rotation rate from zero produces significant changes in the structure of the turbulent flow. Starting with a two-dimensional inverse energy cascade at zero rotation, the flow first transitions to a forward cascade of kinetic energy, then to a shear-layer dominated regime and finally to a second shear-layer regime where the kinetic energy flux is strongly suppressed and the energy transfer is mediated by the induced magnetic field. We show that the first two transitions occur at distinct values of the Rossby number, and the third occurs at a distinct value of the Lehnert number. The three-dimensional results are confirmed using an asymptotic two-dimensional, three-component model, which allows us to extend our results to the planetary-relevant case of an arbitrary angle between the rotation vector and guide field. More generally, our results demonstrate that, when considering the simultaneous limits of strong rotation and a strong guide field, the order in which those limits are taken matters in the misaligned case.

Key words: rotating turbulence, MHD turbulence, bifurcation

† Email address for correspondence: santib@mit.edu

1. Introduction

Turbulence in geophysical and astrophysical settings contains additional physical ingredients that break the isotropy of the flow, a traditional assumption in classical turbulence theory, thereby adding complexity to the system at hand (Frisch 1995; Davidson 2013; Alexakis & Biferale 2018). This includes, but is not limited to, rotating, electrically conducting, stratified and large aspect ratio systems. Asymptotic regimes are sought out to simplify the system, thus allowing previous ideas and techniques of idealized turbulence to be used. This is done by studying the limiting equations as a control parameter (rotation, aspect ratio, etc.) is taken to zero or infinity. For example, one particular success is the quasigeostrophic approximation, which predicts horizontal motion in the presence of stratification and rapid rotation (Charney 1971; Vallis 2017). More generally, in rapidly rotating systems without stratification and with periodic boundary conditions, the flow becomes two-dimensional (2-D), invariant along the rotation axis (Smith & Waleffe 1999; Mininni & Pouquet 2010; Gallet 2015; Buzzicotti *et al.* 2018). A similar simplification occurs in plasmas in the presence of a strong uniform background magnetic 'guiding' field, reducing the dynamics to 2-D magnetohydrodynamics (MHD) (Montgomery & Turner 1981; Nazarenko 2007; Alexakis 2011; Bigot & Galtier 2011; Sujovolsky & Mininni 2016), and further to 2-D hydrodynamics (HD) if the magnetic field is not forced (Alexakis 2011; Sujovolsky & Mininni 2016). Both of these limits produce 2-D HD turbulence, which is characterized by the presence of an inverse cascade of energy, in which energy goes from the forcing scale towards larger scales (Kraichnan 1967; Boffetta & Ecke 2012; Alexakis & Biferale 2018). This is in contrast to the forward energy cascades found in 3-D HD and MHD turbulence in the absence of a guiding field, where energy cascades to smaller scales. The asymptotic regimes allow one to use energy cascade arguments to help understand turbulent geophysical and astrophysical phenomena. For example, the inverse cascade in the quasigeostrophic system is thought to contribute to the formation of jets in rapidly rotating planetary atmospheres (Rhines 1975; Cho & Polvani 1996*a,b*; Held & Larichev 1996; Arbic & Flierl 2004; Tobias, Diamond & Hughes 2007; Gallet & Ferrari 2021). An analogous cascade mechanism is thought to be responsible for the formation of poloidal jets in tokamak plasmas in the presence of a strong background toroidal guiding magnetic field (Diamond *et al.* 2005).

In many geophysical and astrophysical contexts, however, it is expected that a fluid is subject to some combination of rotation, magnetic field, and stratification (Cho 2008; Davidson 2013; Vallis 2017). Asymptotic analysis of these combined cases is more difficult, where often the order in which the limits are taken matters, and knowing which regime is observed in nature (and how the energy cascades behave) is a challenge (Aurnou *et al.* 2015).

Furthermore, real physical systems are not subject to infinite rotation rates or infinite background magnetic field strengths and reality often lies at intermediate values. There is currently no existing theory for the cascade direction of such intermediate parameters, and it is only more recently through state-of-the-art simulations (Smith, Chasnov & Waleffe 1996; Smith & Waleffe 1999; Celani, Musacchio & Vincenzi 2010; Pouquet & Marino 2013; Deusebio *et al.* 2014; Marino, Pouquet & Rosenberg 2015) and laboratory experiments (Xia *et al.* 2011; Campagne *et al.* 2014; Baker *et al.* 2018) that we are able to carefully investigate their turbulent dynamics. These studies looking into the cascade of conserved quantities in geophysical and astrophysical flows have revealed the presence of bidirectional cascades at intermediate parameter values, in which a fraction of the conserved quantity input by the forcing goes to large scales whereas the rest goes to small scales (Alexakis & Biferale 2018; Pouquet *et al.* 2019). This is not to be confused with dual cascade scenarios, where the system has two conserved quadratic

quantities which cascade in different directions, such as in 2-D HD turbulence with the forward cascade of enstrophy and inverse cascade of energy. Most of these geophysical and astrophysical systems seem to form bidirectional cascades at particular critical values of the control parameters. Numerical simulations are crucial in revealing the behaviour of turbulent systems in configurations and parameter values that are out of reach of asymptotic methods.

Here, we investigate the turbulent dynamics of an incompressible electrically conducting MHD fluid subject to rotation and a misaligned uniform background magnetic field using a series of direct numerical simulations. Such a configuration is expected to represent the turbulent dynamics in the atmospheric interiors of gas giant planets in the transition region between the outer, neutral atmosphere and the deep, ionized one (e.g. Liu, Goldreich & Stevenson 2008; Dietrich & Jones 2018; Benavides & Flierl 2020). There, the dynamics is characterized by rapid rotation and the presence of a strong background field generated by the dynamo in the deep interior region below. A simplified case of a dipole magnetic field present in the transition layer would suggest that the alignment between rotation and the background field would vary with latitude. The latest Juno measurements by Moore *et al.* (2018) show, however, that the background field around the transition region is quite 'patchy', but we still expect the misalignment with rotation to be a generic feature. In these regions the electrical conductivity is expected to be quite low (Liu *et al.* 2008; French *et al.* 2012; Dietrich & Jones 2018). For the sake of generality, in the following we investigate a model with rather large conductivity, before discussing how most of the results carry over to the low-conducting case in § 5. To some extent, the ultimate effect of the background magnetic field is the same, resulting in anisotropic flows, and eventually the two-dimensionalization of the flow perpendicular to the field (Sommeria & Moreau 1982; Vorobev *et al.* 2005; Thess & Zikanov 2007; Favier *et al.* 2010; Gallet & Doering 2015; Baker *et al.* 2018). While our interests are at the fundamental level, with application to gas giant planets in mind, the effects of a background field and (possibly misaligned) rotation also need to be considered in the formation and dynamics of ionized protoplanetary disks in the presence of the host star's magnetosphere (Fromang 2005; Armitage 2011; Joos, Hennebelle & Ciardi 2012; Simon *et al.* 2013, 2018). Both of the astrophysical settings mentioned so far are geometrically confined, so we will not explore large domain size effects in this work (see discussion in § 4).

More generally, given the prevalence of astrophysical systems which are both ionized and undergoing rotation, we expect our results to be general enough to apply in other contexts. Our idealized system has simplified forcing and boundary conditions compared with realistic astrophysical settings. However, its role is to uncover the dynamics of the small scales, which can eventually guide parametrizations of sub-grid-scale fluxes in large-scale models of astrophysical objects.

In particular, we are interested in understanding what happens when there are two, two-dimensionalizing effects which act in different directions. What is the fate of the inverse cascade and how 'fragile' is it to the variation in the secondary control parameter? Focusing on the case of a strong background field, we find that increasing the rotation rate from zero produces significant changes in the structure of the turbulent flow. Starting from a 2-D inverse cascade scenario at zero rotation, we find four distinct dynamical regimes as we increase rotation: for weak rotation rates we observe a bidirectional cascade of kinetic energy, with energy flux to large scales decreasing as rotation is increased, and negligible induced magnetic energy. For rotation rates past some critical point, the flow transitions to a purely forward cascade of kinetic energy. Further increasing the rotation rate results in a shear-layer dominated regime, where nonlinearities at large scales are suppressed. Finally, at the largest rotation rates we investigated, we found a second shear-layer regime where

the induced magnetic energy is no longer negligible, the kinetic energy flux is strongly suppressed and the energy transfer is purely mediated by nonlinear terms which include the induced magnetic field. Using a 2-D three-component asymptotic model of our system, we also show that the first three regimes are separated by sharp transitions, hinting at the existence of a bifurcation in the behaviour of the turbulent flow. One is found to be similar to other previously found transitions from a bidirectional cascade to a forward one, while the other shows subcritical behaviour including a discontinuity in the order parameter and hysteresis. The transition to the magnetically active regime is beyond the scope of the reduced model, but we show that it also sharpens towards a critical value as the background magnetic field strength increases. We find more generally that, when considering the limit of strong rotation and strong magnetic field, the order in which those limits are taken matters.

In § 2 we introduce the system we will study: rotating MHD in the presence of a background magnetic field, referred to as $B\Omega$-MHD (Menu, Galtier & Petitdemange 2019). In § 3 we discuss results from 3-D simulations in which the background magnetic field is strong and as we vary the rotation rate in a perpendicular direction. In § 4 we introduce a two-dimensional, three-component (2D3C) asymptotic model (similar to that derived in Montgomery & Turner 1981) representing the strong background magnetic field limit and including rotation, and discuss results from the simulations of that reduced system. Discussion and implications of our results are presented in § 5, where we extend our results to an arbitrary angle between rotation and background magnetic field, before discussing the low conductivity limit, relevant to planetary settings.

2. Rotating MHD in the presence of a background magnetic field

The equations for rotating MHD in the presence of a uniform background magnetic field are (Shebalin 2006; Galtier 2014)

$$\frac{\partial \boldsymbol{v}}{\partial t} + (\boldsymbol{v} \cdot \nabla)\boldsymbol{v} = -\nabla p^* - 2\boldsymbol{\Omega} \times \boldsymbol{v} + (\nabla \times \boldsymbol{b}) \times (\boldsymbol{B_0} + \boldsymbol{b}) + \boldsymbol{D}_v + \boldsymbol{f}, \qquad (2.1)$$

$$\frac{\partial \boldsymbol{b}}{\partial t} + (\boldsymbol{v} \cdot \nabla)\boldsymbol{b} = (\boldsymbol{B_0} \cdot \nabla)\boldsymbol{v} + (\boldsymbol{b} \cdot \nabla)\boldsymbol{v} + \boldsymbol{D}_b, \qquad (2.2)$$

$$\nabla \cdot \boldsymbol{v} = 0, \, \nabla \cdot \boldsymbol{b} = 0, \qquad (2.3)$$

where $\boldsymbol{v} = (v_x, v_y, v_z)$ is the velocity field and $\boldsymbol{b}$ is the induced magnetic field, making up the two dynamical variables in this system. The two control parameters are $\boldsymbol{\Omega}$, the global rotation vector (with magnitude Ω) and $\boldsymbol{B_0}$, the uniform background field (with magnitude B_0). Other definitions include the total pressure modified by rotation p^*, which is normalized by the constant density ρ_0 and the dissipation terms, $\boldsymbol{D}_v$ and $\boldsymbol{D}_b$, which could be regular viscosity and magnetic diffusion, respectively, but might also include other forms of dissipation such as drag or hypodiffusion. The exact form of these terms will be described in § 3, when the simulations are introduced. Magnetic fields are in Alfvén units, being normalized by $\sqrt{\rho_0 \mu_0}$, where μ_0 is the magnetic permeability. Finally, $\boldsymbol{f}$ is a body force, which will be used to inject energy into the velocity field.

The inviscid and perfectly conducting system conserves the total energy,

$$E = \tfrac{1}{2} \int (\boldsymbol{v}^2 + \boldsymbol{b}^2) \, \mathrm{d}^3 x. \qquad (2.4)$$

However, when $\boldsymbol{\Omega}$ and $\boldsymbol{B_0}$ are collinear, this system also conserves what is known as the parallel helicity (Shebalin 2006) or hybrid helicity (Galtier 2014; Menu et al. 2019).

The collinear system has received considerable attention – favoured over the misaligned case in part due to its extra conserved quantity and the potential relevance of its cascade for dynamo action (Shebalin 2006; Menu *et al.* 2019). It also possesses simplified linear wave solutions which have been used to develop a weak wave turbulence theory (Galtier 2014; Bell & Nazarenko 2019). Here, we will not be considering the collinear case, and so only the total energy will be conserved in our study of $B\Omega$-MHD in § 3. Although waves are certainly present in our system, our work concerns the strongly turbulent dynamics of energy cascades (present partly in the zero frequency modes of the system). See Appendix A for the dispersion relation of waves in the misaligned case.

Most studies, with rotation and background magnetic field aligned or not, have focused on how rotation and a moderate background field affect the decay of kinetic and magnetic energies in unforced simulations (Lehnert 1955; Favier, Godeferd & Cambon 2012; Baklouti *et al.* 2019; Bell & Nazarenko 2019). Menu *et al.* (2019) investigated the sensitivity of the cascade of hybrid helicity for various rotation and guide field alignments in forced-dissipative simulations. We consider the effects of rotation and a misaligned background magnetic field on the two-dimensionalization of the flow and the energy cascade, including the limits of strong rotation and strong background magnetic field.

In our study, the rotation and background magnetic field vectors are perpendicular to each other, namely, we have chosen $\boldsymbol{\Omega} = \Omega\hat{\boldsymbol{z}}$ and $\boldsymbol{B_0} = B_0\hat{\boldsymbol{x}}$, the extension to an arbitrary angle between $\boldsymbol{\Omega}$ and $\boldsymbol{B_0}$ being discussed in § 5. The turbulence is maintained at a statistically steady state by a forcing which inputs energy at a mean rate I at a length scale $1/k_f$ (see details in § 3). As a result, there is an emergent velocity scale U defined to be $U^3 \equiv Ik_f^{-1}$, that we compare with the background field as a measure of its strength, the inverse Alfvén Mach number

$$M^{-1} \equiv \frac{B_0}{U}. \tag{2.5}$$

This dimensionless number can also be thought of as a measure of how the third term on the right-hand side of (2.1) (the Lorentz force) and the first term on the right-hand side of (2.2) compare with the advection terms in each respective equation, which would determine whether or not the background field affects the dominant dynamics. When $M^{-1} \gg 1$ the Lorentz force acts to constrain the velocity and induced magnetic fields so that they do not vary along the x-direction and most of the energy lies in the $k_x = 0$ modes, resulting in 2-D MHD (Montgomery & Turner 1981; Nazarenko 2007; Alexakis 2011; Bigot & Galtier 2011; Sujovolsky & Mininni 2016). It is important to note that, while the dynamics depends on y, z and t, all vector components can be non-zero in periodic domains. This is called two-dimensional, three-component (2D3C) dynamics (Biferale, Buzzicotti & Linkmann 2017). If the induced magnetic field is not directly forced (as is the case in our study), this results in 2D3C HD and an inverse cascade of horizontal kinetic energy (Alexakis 2011; Sujovolsky & Mininni 2016). All of our simulations lie in the regime of strong background magnetic field, $M^{-1} \gg 1$, making the rotation rate the main control parameter in our study. Does this asymptotic regime survive in the presence of rotation?

The relative strength of rotation is measured by the inverse Rossby number

$$Ro^{-1} \equiv \frac{2\Omega}{k_f U}. \tag{2.6}$$

This number measures the relative importance of the second term on the right-hand side of (2.1) (the Coriolis force) to the advection term, which would determine whether or not

the rotation affects the dynamics. Unlike the background magnetic field, the Coriolis force only directly affects the velocity field. For non-stratified rapidly rotating HD in the absence of any magnetic field, $Ro^{-1} \gg 1$, the strong Coriolis force acts to constrain the flow such that it does not vary along the z-direction and most of the energy lies in the $k_z = 0$ modes (Smith & Waleffe 1999; Mininni & Pouquet 2010; Gallet 2015; Vallis 2017; Buzzicotti *et al.* 2018), which results in 2D3C HD where the dynamics depends only on x, y, and t. If the fluid is ionized and initialized with a non-zero seed magnetic field, rapid rotation does not necessarily result in 2D3C HD because there is no direct constraint on the induced magnetic field. Instead, if the transverse velocity component does not vanish, rapidly rotating dynamos are formed with z-dependent induced magnetic fields (Otani 1993; Smith & Tobias 2004; Aurnou *et al.* 2015; Seshasayanan & Alexakis 2016*b*; Seshasayanan, Gallet & Alexakis 2017; Tobias 2021). However, since our base state is the x-independent 2D3C HD regime found when $M^{-1} \gg 1$, rapid rotation is expected to act to constrain the flow and prevent it from varying in the z-direction. Note that, in this configuration, rotation is in the plane of the 2-D dynamics, not out of the plane as is often the case when it itself is the cause of the bidimensionalization. Since rotation is now in the plane of the 2-D velocities, the Coriolis force is expected to deflect horizontal velocities out of the plane, as will be discussed in § 4 when we introduce a reduced model for this system following Montgomery & Turner (1981).

Our goal in this study is to investigate the effects that in-plane rotation has on the 2-D flow caused by a strong background magnetic field. In the next section we will describe results from direct numerical simulations of the $B\Omega$-MHD system for various rotation rates, paying particular attention to the resulting energy cascade and morphology of the flow field.

3. Strong background field limit: 3-D $B\Omega$-MHD simulations

Equations (2.1)–(2.3) were solved numerically in a triply periodic domain of side length $2\pi L$ using the Geophysical High-Order Suite for Turbulence (GHOST) code (Mininni *et al.* 2011). The dissipation terms, D_v and D_b, each consist of a 'hyperviscosity' and a large-scale dissipation term called 'hypoviscosity'. The hyperviscosity replaces the regular viscous and magnetic diffusion terms with a Laplacian of a higher order, in our case $\nabla^2 \rightarrow -\nabla^4$. This higher order allows for the possibility of forcing at smaller length scales while still properly resolving the smallest scales at moderate resolutions. As long as the order of the Laplacian is not very large, hyperviscosity has been shown to have no significant effect on the turbulent properties of 3-D turbulence, and we expect the same to be the case for our work (Agrawal *et al.* 2020). The hypoviscosity, which would appear as $\nu_- \nabla^{-2} v$ on the right-hand side of (2.1) and as $\eta_- \nabla^{-2} b$ on the right-hand side of (2.2), acts as a large-scale dissipation term. The resulting expressions for D_v and D_b are,

$$\left.\begin{array}{l} D_v = -\nu\nabla^4 v + \nu_-\nabla^{-2}v, \\ D_b = -\eta\nabla^4 b + \eta_-\nabla^{-2}b, \end{array}\right\} \tag{3.1}$$

where ν is the kinematic 'hyper'-viscosity, $\eta = (\mu_0\sigma)^{-1}$ is the magnetic 'hyper'-diffusivity, σ is the electrical conductivity, ν_- is the 'hypo'-viscosity and η_- is the magnetic 'hypo'-diffusivity. Should an inverse cascade of a conserved quantity occur, this term ensures that no condensate forms, which would otherwise affect the cascades and inertial ranges (Chertkov *et al.* 2007; Xia *et al.* 2008; Gallet & Young 2013; Alexakis & Biferale 2018; Seshasayanan & Alexakis 2018; van Kan & Alexakis 2019). This is done by

System	B_0	M^{-1}	Ω	k_f	Forcing type	ν	ν_-	Resolution	Count
(2.1)–(2.3)	13.3	84	[0–16.6]	8-10	Constant Amplitude	6.6e−7	0.06	256^3	14
(2.1)–(2.3)	6.6	44	[0–7.3]	8-10	Constant Amplitude	6.6e−7	0.06	256^3	11
(2.1)–(2.3)	3.3	23	[0–7.3]	8-10	Constant Amplitude	6.6e−7	0.06	256^3	5
(4.1)–(4.2)	∞	∞	[0–20]	12	Random	4e−7	1.0	512^2	23

Table 1. A summary of the runs performed for this work. All runs have hyper- and hypo-viscosity of the same order (section 3). For runs with a magnetic field, $\mu = \nu$ and $\mu_- = \nu_-$. The simulations used Alfvénic units so that $B_0/\sqrt{\rho_0 \mu_0} \to B_0$ and the other ρ_0 was absorbed into the pressure. The values are non-dimensionalized by L and the forcing amplitude f_0 (or I_0 for random forcing), so that k_f is the forcing mode number and the forcing amplitude (for constant amplitude forcing) or energy injection rate (for the random forcing) are both 1 in these units. The typical velocity, U, was calculated after the fact for each run using $U^3 \equiv I k_f^{-1}$, where $I \equiv \langle \boldsymbol{f} \cdot \boldsymbol{v} \rangle$ is the time- and space-averaged energy injection rate. The count is the number of runs in that set.

choosing the coefficients ν_- and η_- such that the kinetic and magnetic energy at the largest scales is smaller than that of the next largest scales. The modified GHOST code which includes these alternative dissipative terms can be found in a public Github repository (Benavides 2019). It is a standard parallel pseudo-spectral code with a fourth-order Runge–Kutta scheme for time integration and a two-thirds dealiasing rule. The numerical model is non-dimensionalized by L and the forcing amplitude f_0, so that the wavenumbers $\boldsymbol{k}$ correspond to mode numbers of the domain and the forcing amplitude is one. The 3-D forcing $\boldsymbol{f}$ is isotropic and constant in time, comprising of a summation of cosines with wavenumbers in the range $8 < |\boldsymbol{k}| < 10$, making $k_f = 9$, and random phases. The forcing wavenumber range is chosen in an attempt to properly resolve both an inverse cascade and a forward cascade. $I \equiv \langle \boldsymbol{f} \cdot \boldsymbol{v} \rangle$ is the space- and time-averaged energy injection rate, where $\langle \cdot \rangle$ represents a space and time average. We do not force the induced magnetic field.

All runs, unless otherwise stated, are in the large background field regime with $M^{-1} \approx 84$. We find this value to be large enough to produce the expected two-dimensionalization in the absence of rotation (figure 1a). Larger background magnetic field values result in significant restrictions in the time step which would limit our ability to perform the same parameter sweep. The Reynolds and magnetic Reynolds numbers, defined, respectively, as $Re \equiv U/k_f^3 \nu$ and $Re_m \equiv U/k_f^3 \eta$ when considering hyperviscous and hyperdiffusive terms as we do, measure the relative strength of the advection terms compared with the hyperviscous and magnetic hyperdiffusion terms. For the simulations we performed, the Reynolds and magnetic Reynolds numbers were large (approximately 300) and equal to each other, i.e. the magnetic Prandtl number is set to one. We performed 14 runs at $M^{-1} \approx 84$ but at different values of Ro^{-1}, ranging from $Ro^{-1} = 0$ to $Ro^{-1} = 27$. All averages and snapshots were taken in statistically steady states. See table 1 for details of the simulations and a description of how we measured the non-dimensional numbers.

In this study, we are partly concerned with the behaviour of the energy cascade as rotation is varied. We expect the presence of a bidirectional cascade, where a fraction of the energy input by the forcing goes to large scales and the rest goes to small scales. As such, we define a measure for the fraction of energy that goes to large scales in the form of kinetic energy, ε_-, and that which goes to small scales in the form of kinetic energy ε and magnetic energy ε_b. Since the large-scale magnetic energy dissipation is practically zero for every simulation performed, we ignore it from our analysis, as it plays no role. These measures are based on the dissipation rates from each of the three dissipation terms,
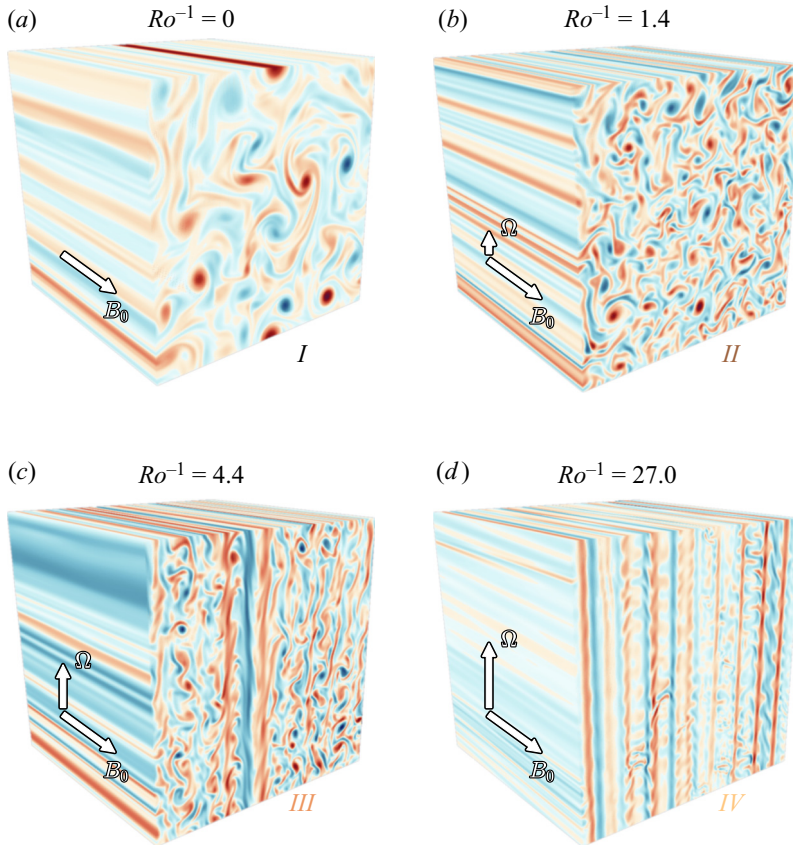
Figure 1. Snapshots of the field-aligned vorticity $\omega = \hat{x} \cdot (\nabla \times \boldsymbol{v})$, representing, from top left to bottom right, Regimes I (*a*), II (*b*), III (*c*) and IV (*d*), as rotation rate is increased. The red colours represent positive vorticity whereas the blue represents negative vorticity. Regime I is characterized by a bidirectional cascade, Regime II a purely forward cascade, Regime III the formation of strong shear layers (seen here in the middle of the domain) and Regime IV magnetically active shear layers. Regimes I–III have a negligible induced magnetic energy, unlike Regime IV whose magnetic energy dominates the dynamics (figure 2).

and are defined in the following way:

$$\varepsilon_{-} \equiv \nu_{-} \langle |\nabla^{-1} \boldsymbol{v}|^2 \rangle / I, \quad \varepsilon \equiv \nu \langle |\nabla^2 \boldsymbol{v}|^2 \rangle / I, \quad \varepsilon_b \equiv \eta \langle |\nabla^2 \boldsymbol{b}|^2 \rangle / I. \quad (3.2a\text{--}c)$$

Energy balance at steady state tells us that $\varepsilon_{-} + \varepsilon + \varepsilon_b = 1$. In the limit of large Reynolds number and large forcing wavenumber, none of the energy injected is dissipated at the forcing scale and proper inertial ranges are formed. In this case, the dissipation rate at large scales represents the fraction of energy cascading to large scales, and similarly for the dissipation rate at small scales. Our runs do not reach these idealized limits. The lack of scale separation between the forcing and large-scale dissipation will manifest itself in two related ways in this paper: (i) the large-scale dissipation rate will remain non-zero despite zero average inverse cascade, because some energy that is being injected at k_f will be dissipated by the large-scale dissipation mechanism ($\varepsilon_{-} \leq 0.1$ for the 3-D runs), and (ii) when layers form in Regime III, both the 3-D runs and 2D3C runs show an increase in large-scale dissipation rate, not because of the presence of an inverse cascade, but because the layers form coherent structures near the forcing scale, their energy grows and hence a stronger large-scale dissipation rate is achieved. These jumps in ε_{-} denote the presence of

935 A1-8

shear layers, as discussed in § 4. To complement these estimates for energy cascades, we will look at the normalized spectral energy flux

$$\Pi_{KE}(k) \equiv \langle \boldsymbol{v}^{<k} \cdot (\boldsymbol{v} \cdot \boldsymbol{\nabla} \boldsymbol{v}) \rangle / I, \tag{3.3}$$

$$\Pi_{ME}(k) \equiv -\langle \boldsymbol{v}^{<k} \cdot ((\boldsymbol{B_0} + \boldsymbol{b}) \cdot \boldsymbol{\nabla} \boldsymbol{b}) \rangle / I + \langle \boldsymbol{b}^{<k} \cdot (\boldsymbol{v} \cdot \boldsymbol{\nabla} \boldsymbol{b} - (\boldsymbol{B_0} + \boldsymbol{b}) \cdot \boldsymbol{\nabla} \boldsymbol{v}) \rangle / I, \tag{3.4}$$

where $\boldsymbol{v}^{<k}$ stands for a filtering of the velocity $\boldsymbol{v}$ in Fourier space so that only the wavenumbers with modulus smaller than k are kept. The flux $\Pi(k)$ expresses the rate at which energy is flowing out of scales larger than $2\pi/k$ due to nonlinear interactions, normalized by the energy injection rate. Therefore, if energy is going from large to small scales, the energy flux will be positive, and *vice versa*. Finally, to quantify the amount and type of energy at each scale, we will also look at the energy spectra

$$E_{KE}(k) \equiv \tfrac{1}{2} \sum_{|\boldsymbol{k}|=k} |\hat{\boldsymbol{v}}|^2(\boldsymbol{k}), \quad E_{ME}(k) \equiv \tfrac{1}{2} \sum_{|\boldsymbol{k}|=k} |\hat{\boldsymbol{b}}|^2(\boldsymbol{k}), \tag{3.5a,b}$$

where $\hat{\boldsymbol{v}}$ denotes the Fourier transform of $\boldsymbol{v}$.

Beginning from quasi-2-D turbulence on the *y–z* plane at zero rotation, we find four distinct regimes as we increased rotation (figure 1). Although not so apparent in the 3-D simulations, these regimes are separated by seemingly sharp transitions, whose boundaries are determined in § 4.

Regime I (figure 1*a*), defined for runs with $Ro^{-1} < 0.6$, is characterized by the presence of a bidirectional cascade. This can be seen in figure 2 as a non-zero large-scale dissipation rate as well as in figure 3(*e*), where the spectral energy transfers show that about half of the energy injected by the forcing goes to large scales (negative $\Pi(k)$) and the other half goes to small scales (positive $\Pi(k)$). The fraction of energy that goes to larger scales decreases with increasing rotation (figure 2). At zero rotation we do not have a purely inverse cascade ($\varepsilon_- \approx 1$) due to a combination of finite background magnetic field strength and, as we will see in § 4, the fact that we are forcing the out-of-plane velocity which acts as a passive scalar in the two-dimensionalized dynamics, thus contributing to a forward energy flux (Campagne *et al.* 2014; Biferale *et al.* 2017). Therefore, at zero rotation rate, the system is undergoing two independent cascades: an inverse energy cascade of horizontal kinetic energy and a forward cascade of the out-of-plane kinetic energy. If we were to force only the horizontal velocity components in the $k_x = 0$ wavenumber plane, we would expect to see $\varepsilon_- \approx 1$ at zero rotation. Figure 3(*a*) shows the kinetic and magnetic energy spectra, which demonstrates that the magnetic energy is orders of magnitude smaller than the kinetic energy (particularly at large scales) and that the largest scales have the most energy, providing further confirmation of the presence of an inverse cascade. The spike of magnetic energy at the forcing scale is due to the excitation of Alfvén waves from the isotropic forcing. The eddy length scales seen in figure 1(*a*) are set by a combination of the energy injection and the large-scale hypoviscosity coefficient. Regime II (figure 1*b*), defined for runs with $0.6 < Ro^{-1} < 2.1$, is characterized by a purely forward cascade of energy (figures 2 and 3*f*). This may come as a surprise, given that the dynamics is two-dimensional. The reason for this seemingly contradictory state is that, while two-dimensional, all three velocity components are active in the dynamics and, furthermore, are coupled together with rotation. This results in a set of reduced 2D3C equations which no longer conserve enstrophy, making a forward cascade of energy possible. The rotating 2D3C system will be discussed and explored numerically in § 4.

Regime III (figure 1*c*), defined for runs with $2.1 < Ro^{-1} < 7.5$, is characterized by the formation of strong shear layers along the *y*-direction, consisting of uniform velocity
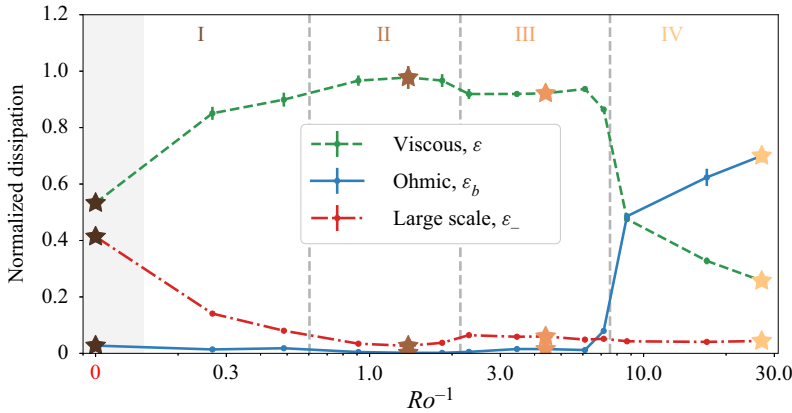
Figure 2. Dissipation rates normalized by the energy injection rate as a function of rotation rate measured by the inverse Rossby number Ro^{-1}. The blue solid line shows the ohmic dissipation rate due to the magnetic diffusion term, ε_b, the green dashed line shows the viscous dissipation rate, ε, and the red dash-dotted line shows the large-scale dissipation rate due to the hypoviscosity, ε_-. Each regime is labelled at the top, and the vertical dashed lines represent boundaries between regimes, chosen based on the 2-D runs in § 4. Stars represent runs whose snapshots are shown in figure 1.
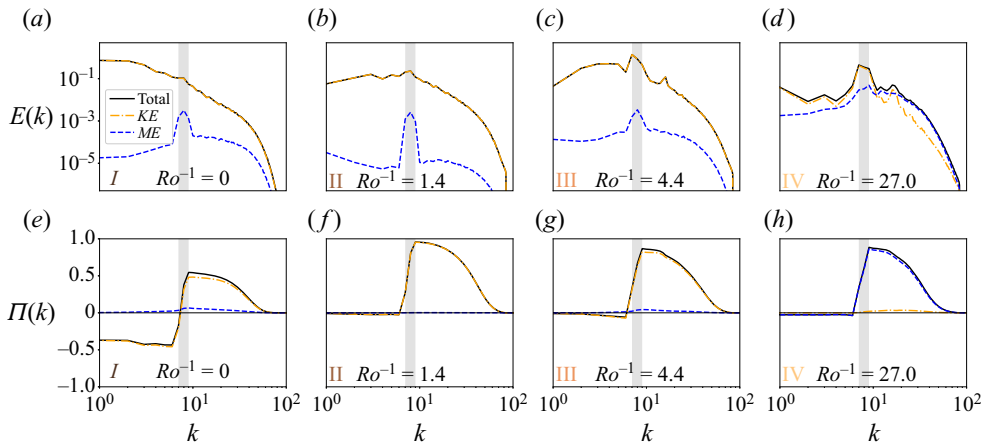
Figure 3. The time-averaged energy spectra (*a-d*) and spectral energy flux (*e-h*) for each regime found in our simulations. The blue dashed line shows the magnetic components, either E_{ME} or Π_{ME}, the orange dash-dotted line shows the kinetic components, E_{KE} or Π_{KE}, and the solid black line shows their sum. The grey box represents the forcing range. These are from the same simulations shown in figure 1 and which are starred in figure 2.

in the *x–z* plane. The shear layers form when the rotational constraint on the dynamics at large scales becomes sufficiently large, requiring that $\partial_z \boldsymbol{v} \approx 0$ at those scales. The combination of $\partial_z = \partial_x = 0$ and incompressibility implies that $v_y = 0$ (since we are in a periodic domain), and thus that the last remaining component of the nonlinear advection term $v_y \partial_y = 0$ and nonlinearities are suppressed at large scales. Because of the suppressed nonlinearity at large scales, these shear layers form coherent structures that are fed directly by the forcing but that do not transfer that energy away, causing a build up of energy (not shown). The energy in the layers builds until a combination of the large-scale dissipation (figure 2) and the nonlinear term (figure 3*g*) are able to remove energy from those scales.

935 A1-10

Regimes I–III have negligible induced magnetic energy, as is observed in simulations of MHD with a strong background field (Alexakis 2011; Sujovolsky & Mininni 2016), and so the induced magnetic field plays an insignificant role in the dynamics. The magnetic fluctuations are also much smaller than B_0 – less than 0.5 % of B_0 in Regimes I–III.

This changes, however, in Regime IV (figure 1*d*), defined for runs with $Ro^{-1} > 7.5$, where we have found the activation and growth of the induced magnetic field, which dominates both the energy as well as the nonlinear energy transfers (figure 2). The nonlinear advection term in the momentum equation is suppressed for practically all scales (figure 3*h*), leading to laminar-like shear-layer structures (figure 1*d*) and a turbulent magnetic field which is responsible for the nonlinear transfers of energy across scales, via the Lorentz force and the magnetic induction equation. The shear-layer spacing in figure 1(*d*) is set by the forcing scale. In this regime, significant induced magnetic field fluctuations occur both parallel and perpendicular to the background magnetic field, with a magnitude of approximately 3 % of B_0.

We expect the boundaries between Regimes I–III to be independent of M^{-1}, as they are part of the asymptotic 2D3C HD, whose sole parameter is the rotation rate. We confirm this in the next section, which deals specifically with this asymptotic set of equations, by showing that the regime transitions happen for the same values of Ro^{-1}. The transition from Regime III to IV is of a different nature and represents a breakdown of the hydrodynamic behaviour found for lower rotation rates. This transition is found to be M^{-1}-dependent, and will be discussed briefly in § 5.

4. Comparison with rotating 2D3C model

Regimes I–III can be better understood by considering the asymptotic limit of (2.1)–(2.3) when taking $M^{-1} \to \infty$ and keeping $Ro^{-1} \sim O(1)$ and the domain size fixed. The choice of keeping the domain size fixed is based on the fact that we are motivated mostly by astrophysical settings in confined geometries, in the presence of a strong background magnetic field. We acknowledge, however, that in many other astrophysical settings, such as the extended atmosphere of stars or the interstellar medium, a confined geometry may not be the best representative system to study. In such systems, a more appropriate limit might include taking the domain size to infinity at the same time as the M^{-1}, so as to prevent the exact two-dimensionalization of the flow (Thess & Zikanov 2007; Gallet & Doering 2015). The limiting equations in this case would resemble more the Reduced MHD system, derived for tokamaks but used also to study some astrophysical systems, in which the flow is highly anisotropic, yet still three-dimensional (Strauss 1976; Oughton, Matthaeus & Dmitruk 2017).

Our limiting procedure, with fixed domain size, is similar to that done in Montgomery & Turner (1981), with the exception that we include the Coriolis term, and so we only briefly discuss it here. Assuming a background magnetic field in the x direction and a rotation axis along the z direction, the process results in a set of three dynamical equations and one nonlinear constraint for the three variables: $\psi(y, z, t)$ the streamfunction for the in-plane velocities, $v_x(y, z, t)$ the out-of-plane velocity and $A(y, z, t)$ the potential for the in-plane magnetic field. This novel constraint, which results from the presence of the Coriolis term, states that either $\delta A / \delta v_x = 0$ or $v_y = \partial_z \psi = 0$, where the former is the functional derivative of A with respect to v_x. Our 3-D simulations from § 3 seem to be consistent with these constraints, where, in Regimes I–III for $Ro^{-1} < 7.5$, we have $A \approx 0$ but $v_y \neq 0$ and, in Regime IV for $Ro^{-1} > 7.5$, we have $A \neq 0$ but $v_y = \partial_z \psi \approx 0$. For the purposes of studying the reduced dynamics of Regimes I–III, we assume $A = 0$,

knowing that it would not capture the transition to Regime IV. The resulting equations form the 2D3C system with in-plane rotation

$$\frac{\partial v_x}{\partial t} + [v_x, \psi] = 2\Omega \frac{\partial \psi}{\partial z} + \nu \nabla_\perp^2 v_x + f_x, \tag{4.1}$$

$$\frac{\partial \omega}{\partial t} + [\omega, \psi] = 2\Omega \frac{\partial v_x}{\partial z} + \nu \nabla_\perp^2 \omega + f_\omega, \tag{4.2}$$

where $[F, G] \equiv \partial_y F \partial_z G - \partial_y G \partial_z F = 0$, $\nabla_\perp = (0, \partial_y, \partial_z)$, $\omega = \hat{x} \cdot (\nabla \times \boldsymbol{v}) = -\nabla_\perp^2 \psi$ is the out-of-plane vorticity (of the in-plane velocities), $\perp$ implies the directions perpendicular to the background magnetic field and $f_\omega = \hat{x} \cdot (\nabla_\perp \times \boldsymbol{f}_\perp)$. One could equivalently arrive at (4.1) and (4.2) by taking rotating 3-D HD and requiring that the velocity field does not depend on x. If considering an arbitrary angle between the background field and rotation, only the perpendicular projection of the rotation vector on the background field enters the model. For example, supposing without loss of generality that $\boldsymbol{B_0} = B_0\hat{x}$ and $\boldsymbol{\Omega} = \Omega(\sin(\theta)\hat{z} + \cos(\theta)\hat{x})$, then the Coriolis terms on the right-hand side of (4.1) and (4.2) will be multiplied by $\sin(\theta)$. This asymptotic model is in the same spirit as some of the magnetized quasigeostrophic models used in astrophysical applications (Aurnou *et al.* 2015; Maffei *et al.* 2019), but it is important to note that here we have taken $M^{-1} \to \infty$ while keeping $Ro^{-1} \sim O(1)$, whereas the magnetized quasigeostrophic models take the rapidly rotating limit first. As is discussed in § 5, these limits are not expected to be the same.

The Coriolis force now couples the two equations together, making what would otherwise be a passive tracer into an active one. In fact, for non-zero rotation, it can be shown that the 2D3C rotating system conserves kinetic energy and helicity

$$KE = \tfrac{1}{2} \int v_x^2 + |\nabla \psi|^2 \, \mathrm{d}^2x, \tag{4.3}$$

$$H = \int v_x \omega \, \mathrm{d}^2x. \tag{4.4}$$

These are the same conserved quantities as in 3-D HD, but we emphasize that the dynamics is two-dimensional and occurs on the y–z plane. This is in contrast to the case of zero rotation, where the system conserves (separately) the in-plane kinetic energy $\int |\nabla \psi|^2 \, \mathrm{d}^2x$ and the out-of-plane kinetic energy $\int v_x^2 \, \mathrm{d}^2x$, as well as the enstrophy, $\int \omega^2 \, \mathrm{d}^2x$. The conservation of enstrophy can be shown to prevent the existence of a forward cascade of in-plane kinetic energy (Fjortoft 1953; Kraichnan 1967; Alexakis & Biferale 2018). Without the restriction of enstrophy conservation, though, the kinetic energy may go downscale in a forward cascade, even if one does not force the out-of-plane component.

We solve (4.1) and (4.2), with modified hyper- and hypo-viscosities as in the 3-D simulations, numerically in a doubly periodic domain of side length $2\pi L$ using the 2-D predecessor of GHOST. The code can be found in a public Github repository (Benavides 2020). Unlike the 3-D runs, whose forcing function had a constant amplitude in time, the 2D3C runs have random (white-in-time) forcing. At each time step, a wavenumber $\boldsymbol{k_r}$ of magnitude k_f is chosen at random and $\hat{f}_\omega(\boldsymbol{k})$ (Fourier transform of f_ω) is set to zero everywhere except for at $\boldsymbol{k_r}$, where it had a magnitude $k_f\sqrt{2I_0/\Delta t}$ (Chan, Mitra & Brandenburg 2012). This has the effect of setting the energy injection rate for the in-plane flow to be $I = \langle \psi f_\omega \rangle = I_0$ on average, with I_0 being an input parameter of the simulation. The same forcing is applied for f_x, but with an amplitude of $\sqrt{2I_0/\Delta t}$ instead,
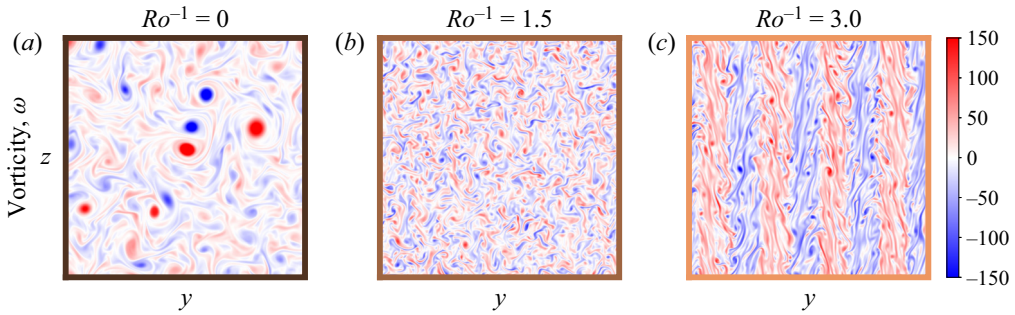
Figure 4. Snapshots of the out-of-plane vorticity, $\omega = \hat{x} \cdot (\nabla \times \boldsymbol{v}) = -\nabla_\perp^2 \psi$, for the 2D3C rotating simulations, representing, from left to right, Regimes I (*a*), II (*b*) and III (*c*), as rotation is increased. We see striking similarities to figure 1, confirming that the asymptotic 2D3C model captures the different regimes found in the 3-D simulations of § 3.

giving the same results. Therefore, half of the energy is injected into the in-plane flow and the other half in the out-of-plane velocity. We non-dimensionalize all dynamical variables as before, using L and now the energy injection rate parameter I_0. For all of the runs reported $k_f = 12$. See table 1 for details on the runs.

The goal of these simulations is to reproduce the parameter sweep performed in § 3, but with the added advantage of working with a 2-D code, thus allowing a larger quantity of runs, higher resolutions (larger Reynolds numbers, around 600) and longer time integration. We have performed 23 runs, with Ro^{-1} ranging from 0 to approximately 5, at four times the horizontal resolution. Our results confirm the presence of Regimes I–III, going from a bidirectional cascade to a forward cascade to a shear-layer configuration (figure 4).

At zero rotation we see a bidirectional cascade with half of the injected energy going to large scales and half going to small scales (figure 5), similar to what was found in the 3-D runs (figure 2). For the 2D3C rotating system this is the case because of the choice of forcing, which injects half of the energy to the in-plane flow and the other half to the out-of-plane velocity. Since the two flows are completely decoupled at zero rotation, they each follow the standard behaviour observed in 2-D and passive tracer turbulence, that is, an inverse and forward cascade of energy, respectively. As we increase rotation, the Coriolis force couples the two fields, enstrophy is no longer conserved, and the in-plane velocities no longer cascade all the injected energy to large scales, resulting in a bidirectional cascade with decreasing inverse energy flux. There is an approximately linear approach to zero inverse energy flux, and at $Ro^{-1} \approx 0.6$ there is a transition to a purely forward cascade. With a larger number of simulations, Regimes I and II are much more clearly separated, and their transition appears to be sharp (figure 5). This transition is qualitatively similar to other bidirectional to forward cascade transitions seen in other studies and could hint at a universal mechanism responsible for this transition (Seshasayanan, Benavides & Alexakis 2014; Seshasayanan & Alexakis 2016*a*; Benavides & Alexakis 2017; van Kan & Alexakis 2020).

Upon further increase of the rotation, the forward cascade regime (Regime II) transitions to a shear-layer configuration (figure 4*c*), entering Regime III. This corresponds to the case when the Coriolis force dominates at large scales, making the dominant balance in (4.1) and (4.2) $\partial_z \psi \approx \partial_z v_x \approx 0$, hence the layers. There are a few differences in the morphology of the shear layers seen for these runs, compared with Regime III in the 3-D simulations (figure 1*c*). Here they take up the whole domain and also appear to equilibrate
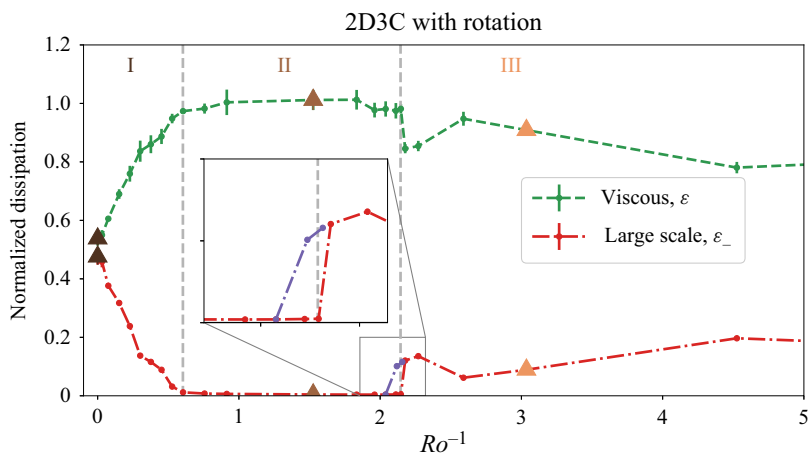
Figure 5. Dissipation rates normalized by the energy injection rate as a function of rotation rate measured by the inverse Rossby number Ro^{-1}. The green dashed line shows the viscous dissipation rate, ε, the red dash-dotted line shows the large-scale dissipation rate due to the hypoviscosity, ε_- and the purple dash-dotted line shows the same but for hysteresis runs initialized with layers. Each regime is labelled at the top, and the vertical dashed lines represent boundaries between regimes. These denoted boundaries are placed at the same value of Ro^{-1} as those seen in figure 2. Triangles represent runs whose snapshots are shown in figure 4.

at scales larger than the forcing, through a series of mergers (not shown). Neither of these characteristics are seen in the shear layers of the 3-D simulations. We believe this is due to a few factors, including the longer integration times and the change in forcing. A surprising feature of this transition, revealed by the better-resolved parameter sweep, is that it is discontinuous (figure 5). (An increase in large-scale dissipation marks this transition not because an inverse cascade forms (a weakness of this measure), but because of a lack of separation of scales. The layers form at or near the forcing scale and remain there as coherent structures, fed directly by the forcing, resulting in a build up of energy at those scales. This, in turn, results in a larger dissipation rate from the large-scale dissipation. If we were to perform runs at a larger k_f, this effect would disappear. The discontinuous transition is also observed in the kinetic energy, which is not shown.) Discontinuities are a characteristic of subcritical bifurcations, which should also display hysteresis. By initializing in the layered regime, we confirmed the presence of hysteresis as we reduced the rotation rate (figure 5 inset).

Despite differences in the forcing, Reynolds numbers and values of M^{-1}, the regime transitions seem to occur for the same values of Ro^{-1}, suggesting that the rotating 2D3C system successfully describes the dynamics observed in the 3-D simulations from § 3 and that Regimes I–III are robust properties of the system. The 2-D asymptotic system has allowed us to perform a more detailed parameter sweep of this parameter space, and has revealed sharp transitions and non-trivial behaviour near those transitions which we did not anticipate from the 3-D simulations.

5. Discussion and conclusions

We have investigated the turbulent dynamics of rotating MHD in the presence of a strong uniform background magnetic field perpendicular to the rotation axis. Our investigations have revealed surprising behaviour, confirmed both by a 3-D model and 2D3C asymptotic model, as rotation rate is increased. We observed the weakening of the inverse cascade,

a transition to a purely forward cascade for relatively weak rotation, and eventually a shear-layer regime at larger rotation rates. These results were obtained in a specific situation: orthogonal rotation and guide field at unit magnetic Prandtl number. However, the derivation of the asymptotic 2D3C model allows us to generalize Regimes I–III to the more realistic situation of an arbitrary angle between rotation and guide field at low magnetic Reynolds number. First, for an arbitrary angle θ between rotation vector and guide field, the reduced model is given by (4.1) and (4.2) where 2Ω is replaced by $2\Omega \sin(\theta)$, the consequence being that the results in figure 5 carry over with Ro^{-1} replaced by $Ro^{-1} \sin(\theta)$ in the x-axis. Second, the 2D3C model illustrates the asymptotic limit in which the guide field is so strong that it prevents any x-dependence. The same phenomenon arises for the low magnetic Reynolds numbers that characterize transitions regions in planetary interiors, see Gallet & Doering (2015) for a rigorous proof in an idealized setting. The consequence is that we expect the very same reduced 2D3C model to hold at low magnetic Reynolds number, starting either from the full MHD equations or from their low magnetic Reynolds number quasi-static approximation. We thus conclude that Regimes I–III carry over to the planetary relevant situation of an arbitrary angle between rotation and guide field, together with a low magnetic Reynolds number (by contrast, the magnetically active Regime IV will be affected by changes in magnetic Prandtl number).

We should also stress the fact that our study focuses on finite-size domains: motivated by transitional layers in planetary interiors, we have restricted attention to a numerical domain that is finite both along the direction of the rotation vector and the local direction of the large-scale magnetic field. By contrast, an idealized turbulent cloud allowed to develop arbitrarily large structures would never achieve exact two-dimensionalization (Davidson 2013; van Kan & Alexakis 2020, 2021), and it is possible that in those cases the Reduced MHD description might be more relevant (Strauss 1976; Oughton *et al.* 2017).

The strong sensitivity of the inverse cascade to in-plane rotation could have significant implications for the morphology of astrophysical flows, which often have both rotation and a background magnetic field. Even for relatively weak rotation ($Ro^{-1} \sim 1$) the inverse cascade is entirely suppressed. As an inverse cascade is considered to be necessary for the formation of jets on gas giant planets, this phenomenon could be a tentative alternative explanation for the weakening of the jets in the depths of their atmospheres, as seen by the Juno mission on Jupiter (Kaspi *et al.* 2018). In the outer electrically neutral regions the jets can form because of the rapid rotation. These rotation-aligned jets may penetrate deep into the interior until they reach the low Re_m ionized regions of the atmosphere whose turbulent dynamics suppresses the jets via ohmic dissipation (Liu *et al.* 2008). Our work reveals another potential alternative, where a misalignment of the rotation and background field cause the localized turbulent dynamics to cascade energy forward instead of inversely, thereby taking away the dynamical origin of the jets. Apart from the astrophysical implications, the rotating 2D3C model might be of interest to those studying phase transitions in turbulence (Alexakis & Biferale 2018) – particularly those interested in the transition from a forward to a bidirectional cascade, since, as far as we are aware, this model is the only 2-D hydrodynamical one with this behaviour.

At the largest rotation rotates, our 3-D simulations showed a sudden activation of the induced magnetic field, signalling the breakdown of the purely hydrodynamic asymptotic model. The velocity field remained 2D3C, but the dynamics differed significantly from the hydrodynamic shear-layer regime and were dominated by an induced 3-D magnetic field. Although the 2D3C model breaks down, given the three-dimensionality of the magnetic field, it is possible this transition could be studied with the Reduced MHD system (Strauss 1976; Oughton *et al.* 2017). A series of simulations at lower M^{-1} values (table 1)
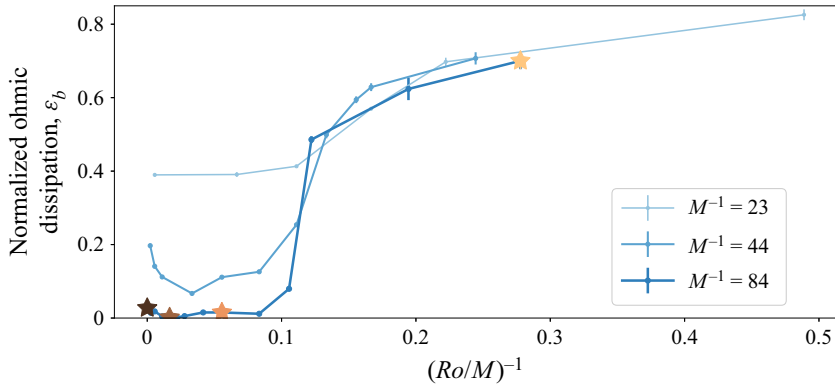
Figure 6. Normalized ohmic dissipation, ε_b, vs $(Ro/M)^{-1}$. The ohmic dissipation represents a measure of how active the induced magnetic field is in the dynamics. We see that, for three values of M^{-1}, the induced magnetic field begins to dominate the dynamics once $(Ro/M)^{-1} > 0.1$, in other words when $Ro^{-1} > 0.1M^{-1}$; $(Ro/M)^{-1}$ is also referred to as the Lehnert number (Lehnert 1955). Stars represent runs whose snapshots are shown in figure 1.

reveals that the transition happens when $M \sim Ro$, which represents roughly the point at which the inertial wave frequency begins to dominate over the Alfvén wave frequency (figure 6, Appendix A). Interestingly, this transition sharpens towards a critical value as the background magnetic field strength increases. Therefore, when considering the limit of strong rotation and strong background magnetic field, the order in which those limits are taken matters. If $Ro^{-1} < 0.1M^{-1}$, then one would expect a hydrodynamical regime, whereas if $Ro^{-1} > 0.1M^{-1}$ a magnetically dominated regime is expected.

Author ORCIDs.
 Santiago J. Benavides https://orcid.org/0000-0002-2281-5695;
 Keaton J. Burns https://orcid.org/0000-0003-4761-4766;
 Basile Gallet https://orcid.org/0000-0002-4366-3889;
 James Y-K. Cho https://orcid.org/0000-0002-4525-5651.

Appendix A. Wave dispersion relation

In the inviscid, perfectly conducting, and force-free case, the linearized $B\Omega$-MHD system admits wave solutions. Taking v of the form $v = \hat{v} \exp i(k \cdot x - \omega t)$ and plugging this into
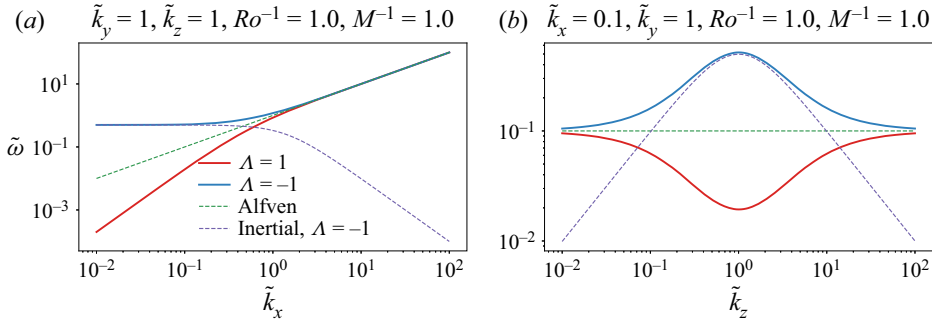
Figure 7. The dispersion relation for waves in the $B\Omega$-MHD system, in the case where $\boldsymbol{B_0} = B_0\hat{\boldsymbol{x}}$ and $\boldsymbol{\Omega} = \Omega\hat{\boldsymbol{z}}$ ((A3)). The green dashed line shows the Alfvén wave dispersion relation, and the purple dashed line shows that of an inertial wave. The low frequency branch with $\Lambda = 1$ is similar to the magnetostrophic mode in the case when $\boldsymbol{B_0}$ and $\boldsymbol{\Omega}$ are aligned (Galtier 2014).

the linearized versions of (2.1)–(2.3), after some algebra we end up with

$$\omega^2(\boldsymbol{k} \times \hat{\boldsymbol{v}}) = 2\mathrm{i}\omega(\boldsymbol{k} \cdot \boldsymbol{\Omega})\hat{\boldsymbol{v}} + (\boldsymbol{k} \cdot \boldsymbol{B_0})^2 \boldsymbol{k} \times \hat{\boldsymbol{v}}. \tag{A1}$$

Next, we introduce the helical orthonormal basis for $\hat{\boldsymbol{v}}$, $\hat{\boldsymbol{v}}(\boldsymbol{k}) = v_k^+ \hat{\boldsymbol{h}}_k^+ + v_k^- \hat{\boldsymbol{h}}_k^-$, where $\boldsymbol{k} \times \hat{\boldsymbol{h}}_k^\Lambda = -\mathrm{i}\Lambda|\boldsymbol{k}|\hat{\boldsymbol{h}}_k^\Lambda$ and $\Lambda = \pm 1$ indicates the sign of the helicity of $\hat{\boldsymbol{h}}_k^\Lambda$ (Herring 1974; Alexakis 2017). Introducing these bases and dotting (A1) with $\hat{\boldsymbol{h}}_k^\Lambda$ we arrive at the dispersion relation. We normalize the frequency with the eddy turnover frequency, $k_f U$, and the wavevector $\boldsymbol{k}$ with k_f, resulting in our final expression for the dispersion relation

$$\tilde{\omega}(\tilde{\boldsymbol{k}}; \Lambda) = -\frac{1}{2}\frac{\tilde{\boldsymbol{k}} \cdot \hat{\boldsymbol{x}}_\parallel^\Omega}{\Lambda \tilde{k} Ro} \pm \frac{1}{2}\sqrt{\left(\frac{\tilde{\boldsymbol{k}} \cdot \hat{\boldsymbol{x}}_\parallel^\Omega}{\tilde{k} Ro}\right)^2 + 4\left(\frac{\tilde{\boldsymbol{k}} \cdot \hat{\boldsymbol{x}}_\parallel^{B_0}}{M}\right)^2}, \tag{A2}$$

where $\tilde{k} \equiv (\tilde{k}_x^2 + \tilde{k}_y^2 + \tilde{k}_z^2)^{1/2}$, $\tilde{k}_i \equiv k_i/k_f$ and $\tilde{\omega} \equiv \omega/(k_f U)$. In the specific case of our study, where $\boldsymbol{B_0} = B_0\hat{\boldsymbol{x}}$ and $\boldsymbol{\Omega} = \Omega\hat{\boldsymbol{z}}$, this simplifies to

$$\tilde{\omega}(\tilde{\boldsymbol{k}}; \Lambda) = -\frac{1}{2}\frac{\tilde{k}_z}{\Lambda \tilde{k} Ro} \pm \frac{1}{2}\sqrt{\left(\frac{\tilde{k}_z}{\tilde{k} Ro}\right)^2 + 4\left(\frac{\tilde{k}_x}{M}\right)^2}. \tag{A3}$$

See figure 7 for a visualization of this dispersion relation, which depends on $\tilde{k}_x$, $\tilde{k}_z$ and $\tilde{k}$.

REFERENCES

AGRAWAL, R., ALEXAKIS, A., BRACHET, M.E. & TUCKERMAN, L.S. 2020 Turbulent cascade, bottleneck, and thermalized spectrum in hyperviscous flows. *Phys. Rev. Fluids* **5**, 024601.

ALEXAKIS, A. 2011 Two-dimensional behavior of three-dimensional magnetohydrodynamic flow with a strong guiding field. *Phys. Rev.* E **84**, 056330.

ALEXAKIS, A. 2017 Helically decomposed turbulence. *J. Fluid Mech.* **812**, 752–770.

ALEXAKIS, A. & BIFERALE, L. 2018 Cascades and transitions in turbulent flows. *Phys. Rep.* **767-769**, 1–101.

ARBIC, B.K. & FLIERL, G.R. 2004 Effects of mean flow direction on energy, isotropy, and coherence of baroclinically unstable beta-plane geostrophic turbulence. *J. Phys. Oceanogr.* **34** (1), 77–93.

ARMITAGE, P.J. 2011 Dynamics of protoplanetary disks. *Annu. Rev. Astron. Astrophys.* **49** (1), 195–236.

AURNOU, J.M., CALKINS, M.A., CHENG, J.S., JULIEN, K., KING, E.M., NIEVES, D., SODERLUND, K.M. & STELLMACH, S. 2015 Rotating convective turbulence in earth and planetary cores. *Phys. Earth Planet. Inter.* **246**, 52–71.

BAKER, N.T., POTHÉRAT, A., DAVOUST, L. & DEBRAY, F. 2018 Inverse and direct energy cascades in three-dimensional magnetohydrodynamic turbulence at low magnetic Reynolds number. *Phys. Rev. Lett.* **120**, 224502.

BAKLOUTI, F.S., KHLIFI, A., SALHI, A., GODEFERD, F., CAMBON, C. & LEHNER, T. 2019 Kinetic-magnetic energy exchanges in rotating magnetohydrodynamic turbulence. *J. Turbul.* **20** (4), 263–284.

BELL, N.K. & NAZARENKO, S.V. 2019 Rotating magnetohydrodynamic turbulence. *J. Phys. A: Math. Theor.* **52** (44), 445501.

BENAVIDES, S.J. 2019 *Geophysical high-order suite for turbulence*. GitHub Repository. Available at: https://github.com/s-benavides/GHOST/tree/pre-release-2, Commit: 2caaa43aad8b9378ec154bfbc26e4c 85d947a4cc.

BENAVIDES, S.J. 2020 *Rot2d3c*. GitHub repository. Available at: https://github.com/s-benavides/Rot2D3C, Commit: 2d511888b78c451fc7b26352916a6ff40ee98b93.

BENAVIDES, S.J. & ALEXAKIS, A. 2017 Critical transitions in thin layer turbulence. *J. Fluid Mech.* **822**, 364–385.

BENAVIDES, S.J. & FLIERL, G.R. 2020 Two-dimensional partially ionized magnetohydrodynamic turbulence. *J. Fluid Mech.* **900**, A28.

BIFERALE, L., BUZZICOTTI, M. & LINKMANN, M. 2017 From two-dimensional to three-dimensional turbulence through two-dimensional three-component flows. *Phys. Fluids* **29** (11), 111101.

BIGOT, B. & GALTIER, S. 2011 Two-dimensional state in driven magnetohydrodynamic turbulence. *Phys. Rev. E* **83**, 026405.

BOFFETTA, G. & ECKE, R.E. 2012 Two-dimensional turbulence. *Annu. Rev. Fluid Mech.* **44** (1), 427–451.

BUZZICOTTI, M., ALUIE, H., BIFERALE, L. & LINKMANN, M. 2018 Energy transfer in turbulence under rotation. *Phys. Rev. Fluids* **3**, 034802.

CAMPAGNE, A., GALLET, B., MOISY, F. & CORTET, P.-P. 2014 Direct and inverse energy cascades in a forced rotating turbulence experiment. *Phys. Fluids* **26** (12), 125112.

CELANI, A., MUSACCHIO, S. & VINCENZI, D. 2010 Turbulence in more than two and less than three dimensions. *Phys. Rev. Lett.* **104**, 184506.

CHAN, C.-K., MITRA, D. & BRANDENBURG, A. 2012 Dynamics of saturated energy condensation in two-dimensional turbulence. *Phys. Rev. E* **85**, 036315.

CHARNEY, J.G. 1971 Geostrophic turbulence. *J. Atmos. Sci.* **28** (6), 1087–1095.

CHERTKOV, M., CONNAUGHTON, C., KOLOKOLOV, I. & LEBEDEV, V. 2007 Dynamics of energy condensation in two-dimensional turbulence. *Phys. Rev. Lett.* **99**, 084501.

CHO, J.Y-K. 2008 Atmospheric dynamics of tidally synchronized extrasolar planets. *Phil. Trans. R. Soc. A: Math. Phys. Engng Sci.* **366** (1884), 4477–4488.

CHO, J.Y-K. & POLVANI, L.M. 1996*a* The emergence of jets and vortices in freely evolving, shallow-water turbulence on a sphere. *Phys. Fluids* **8** (6), 1531–1552.

CHO, J.Y-K. & POLVANI, L.M. 1996*b* The morphogenesis of bands and zonal winds in the atmospheres on the giant outer planets. *Science* **273** (5273), 335–337.

DAVIDSON, P.A. 2013 *Turbulence in Rotating, Stratified and Electrically Conducting Fluids*. Cambridge University Press.

DEUSEBIO, E., BOFFETTA, G., LINDBORG, E. & MUSACCHIO, S. 2014 Dimensional transition in rotating turbulence. *Phys. Rev. E* **90**, 023005.

DIAMOND, P.H., ITOH, S.-I., ITOH, K. & HAHM, T.S. 2005 Zonal flows in plasma–a review. *Plasma Phys. Control. Fusion* **47** (5), R35–R161.

DIETRICH, W & JONES, C.A. 2018 Anelastic spherical dynamos with radially variable electrical conductivity. *Icarus* **305**, 15–32.

FAVIER, B.F.N., GODEFERD, F.S. & CAMBON, C. 2012 On the effect of rotation on magnetohydrodynamic turbulence at high magnetic Reynolds number. *Geophys. Astrophys. Fluid Dyn.* **106** (1), 89–111.

FAVIER, B., GODEFERD, F.S., CAMBON, C. & DELACHE, A. 2010 On the two-dimensionalization of quasistatic magnetohydrodynamic turbulence. *Phys. Fluids* **22** (7), 075104.

FJORTOFT, R. 1953 On the changes in the spectral distribution of kinetic energy for twodimensional, nondivergent flow. *Tellus* **5** (3), 225–230.

FRENCH, M., BECKER, A., LORENZEN, W., NETTELMANN, N., BETHKENHAGEN, M., WICHT, J. & REDMER, R. 2012 Ab initio simulations for material properties along the jupiter adiabat. *Astrophys. J. Suppl. Ser.* **202** (1), 5.

FRISCH, U. 1995 *Turbulence: The Legacy of AN Kolmogorov*. Cambridge University Press.

FROMANG, S. 2005 The effect of MHD turbulence on massive protoplanetary disk fragmentation. *Astron. Astrophys.* **441** (1), 1–8.

GALLET, B. 2015 Exact two-dimensionalization of rapidly rotating large-Reynolds-number flows. *J. Fluid Mech.* **783**, 412–447.

GALLET, B. & DOERING, C.R. 2015 Exact two-dimensionalization of low-magnetic-Reynolds-number flows subject to a strong magnetic field. *J. Fluid Mech.* **773**, 154–177.

GALLET, B. & FERRARI, R. 2021 A quantitative scaling theory for meridional heat transport in planetary atmospheres and oceans. *AGU Adv.* **2** (3), e2020AV000362.

GALLET, B. & YOUNG, W.R. 2013 A two-dimensional vortex condensate at high Reynolds number. *J. Fluid Mech.* **715**, 359–388.

GALTIER, S. 2014 Weak turbulence theory for rotating magnetohydrodynamics and planetary flows. *J. Fluid Mech.* **757** (6), 114–154.

HELD, I.M. & LARICHEV, V.D. 1996 A scaling theory for horizontally homogeneous, baroclinically unstable flow on a beta plane. *J. Atmos. Sci.* **53** (7), 946–952.

HERRING, J.R. 1974 Approach of axisymmetric turbulence to isotropy. *Phys. Fluids* **17** (5), 859–872.

JOOS, M., HENNEBELLE, P. & CIARDI, A. 2012 Protostellar disk formation and transport of angular momentum during magnetized core collapse. *Astron. Astrophys.* **543**, A128.

VAN KAN, A. & ALEXAKIS, A. 2019 Condensates in thin-layer turbulence. *J. Fluid Mech.* **864**, 490–518.

VAN KAN, A. & ALEXAKIS, A. 2020 Critical transition in fast-rotating turbulence within highly elongated domains. *J. Fluid Mech.* **899**, A33.

VAN KAN, A. & ALEXAKIS, A. 2021 Energy cascades in rapidly rotating and stratified turbulence within elongated domains. arXiv:2106.06973.

KASPI, Y., *et al.* 2018 Jupiter's atmospheric jet streams extend thousands of kilometres deep. *Nature* **555**, 223.

KRAICHNAN, R.H. 1967 Inertial ranges in two-dimensional turbulence. *Phys. Fluids* **10** (7), 1417–1423.

LEHNERT, B. 1955 The decay of magneto-turbulence in the presence of a magnetic field and coriolis force. *Q. Appl. Maths* **12** (4), 321–341.

LIU, J., GOLDREICH, P. & STEVENSON, D.J. 2008 Constraints on deep-seated zonal winds inside Jupiter and Saturn. *Icarus* **196** (2), 653–664.

MAFFEI, S., CALKINS, M.A., JULIEN, K. & MARTI, P. 2019 Magnetic quenching of the inverse cascade in rapidly rotating convective turbulence. *Phys. Rev. Fluids* **4**, 041801.

MARINO, R., POUQUET, A. & ROSENBERG, D. 2015 Resolving the paradox of oceanic large-scale balance and small-scale mixing. *Phys. Rev. Lett.* **114**, 114504.

MENU, M.D., GALTIER, S. & PETITDEMANGE, L. 2019 Inverse cascade of hybrid helicity in $b\Omega$-MHD turbulence. *Phys. Rev. Fluids* **4**, 073701.

MININNI, P.D. & POUQUET, A. 2010 Rotating helical turbulence. I. Global evolution and spectral behavior. *Phys. Fluids* **22** (3), 035105.

MININNI, P.D., ROSENBERG, D., REDDY, R. & POUQUET, A. 2011 A hybrid MPI–openmp scheme for scalable parallel pseudospectral computations for fluid turbulence. *Parallel. Comput.* **37** (6), 316–326.

MONTGOMERY, D. & TURNER, L. 1981 Anisotropic magnetohydrodynamic turbulence in a strong external magnetic field. *Phys. Fluids* **24** (5), 825–831.

MOORE, K.M., *et al.* 2018 A complex dynamo inferred from the hemispheric dichotomy of Jupiter's magnetic field. *Nature* **561** (7721), 76–78.

NAZARENKO, S. 2007 2D enslaving of MHD turbulence. *New J. Phys.* **9** (8), 307.

OTANI, N.F. 1993 A fast kinematic dynamo in two-dimensional time-dependent flows. *J. Fluid Mech.* **253**, 327–340.

OUGHTON, S., MATTHAEUS, W.H. & DMITRUK, P. 2017 Reduced MHD in astrophysical applications: Two-dimensional or three-dimensional? *Astrophys. J.* **839** (1), 2.

POUQUET, A. & MARINO, R. 2013 Geophysical turbulence and the duality of the energy flow across scales. *Phys. Rev. Lett.* **111**, 234501.

POUQUET, A., ROSENBERG, D., STAWARZ, J.E. & MARINO, R. 2019 Helicity dynamics, inverse, and bidirectional cascades in fluid and magnetohydrodynamic turbulence: A brief review. *Earth Space Sci.* **6** (3), 351–369.

RHINES, P.B. 1975 Waves and turbulence on a beta-plane. *J. Fluid Mech.* **69** (3), 417–443.

SESHASAYANAN, K. & ALEXAKIS, A. 2016*a* Critical behavior in the inverse to forward energy transition in two-dimensional magnetohydrodynamic flow. *Phys. Rev. E* **93** (1), 013104.

SESHASAYANAN, K. & ALEXAKIS, A. 2016*b* Turbulent 2.5-dimensional dynamos. *J. Fluid Mech.* **799**, 246–264.

SESHASAYANAN, K. & ALEXAKIS, A. 2018 Condensates in rotating turbulent flows. *J. Fluid Mech.* **841**, 434–462.

SESHASAYANAN, K., BENAVIDES, S.J. & ALEXAKIS, A. 2014 On the edge of an inverse cascade. *Phys. Rev. E - Stat. Nonlinear Soft Matt. Phys.* **90** (5), 1–5.

SESHASAYANAN, K., GALLET, B. & ALEXAKIS, A. 2017 Transition to turbulent dynamo saturation. *Phys. Rev. Lett.* **119**, 204503.

SHEBALIN, J.V. 2006 Ideal homogeneous magnetohydrodynamic turbulence in the presence of rotation and a mean magnetic field. *J. Plasma Phys.* **72** (4), 507–524.

SIMON, J.B., BAI, X.-N., ARMITAGE, P.J., STONE, J.M. & BECKWITH, K. 2013 Turbulence in the outer regions of protoplanetary disks. II. Strong accretion driven by a vertical magnetic field. *Astrophys. J.* **775** (1), 73.

SIMON, J.B., BAI, X.-N., FLAHERTY, K.M. & HUGHES, A.M. 2018 Origin of weak turbulence in the outer regions of protoplanetary disks. *Astrophys. J.* **865** (1), 10.

SMITH, L.M., CHASNOV, J.R. & WALEFFE, F. 1996 Crossover from two- to three-dimensional turbulence. *Phys. Rev. Lett.* **77**, 2467–2470.

SMITH, S.G.L. & TOBIAS, S.M. 2004 Vortex dynamos. *J. Fluid Mech.* **498**, 1–21.

SMITH, L.M. & WALEFFE, F. 1999 Transfer of energy to two-dimensional large scales in forced, rotating three-dimensional turbulence. *Phys. Fluids* **11** (6), 1608–1622.

SOMMERIA, J. & MOREAU, R. 1982 Why, how, and when, mhd turbulence becomes two-dimensional. *J. Fluid Mech.* **118**, 507–518.

STRAUSS, H.R. 1976 Nonlinear, three-dimensional magnetohydrodynamics of noncircular tokamaks. *Phys. Fluids* **19** (1), 134–140.

SUJOVOLSKY, N.E. & MININNI, P.D. 2016 Tridimensional to bidimensional transition in magnetohydrodynamic turbulence with a guide field and kinetic helicity injection. *Phys. Rev. Fluids* **1**, 054407.

THESS, A. & ZIKANOV, O. 2007 Transition from two-dimensional to three-dimensional magnetohydrodynamic turbulence. *J. Fluid Mech.* **579**, 383–412.

TOBIAS, S.M. 2021 The turbulent dynamo. *J. Fluid Mech.* **912**, P1.

TOBIAS, S.M., DIAMOND, P.H. & HUGHES, D.W. 2007 β-plane magnetohydrodynamic turbulence in the solar tachocline. *Astrophys. J.* **667**, 113–116.

VALLIS, G.K. 2017 *Atmospheric and Oceanic Fluid Dynamics*. Cambridge University Press.

VOROBEV, A., ZIKANOV, O., DAVIDSON, P.A. & KNAEPEN, B. 2005 Anisotropy of magnetohydrodynamic turbulence at low magnetic Reynolds number. *Phys. Fluids* **17** (12), 125105.

XIA, H., BYRNE, D., FALKOVICH, G. & SHATS, M. 2011 Upscale energy transfer in thick turbulent fluid layers. *Nat. Phys.* **7** (4), 321–324.

XIA, H., PUNZMANN, H., FALKOVICH, G. & SHATS, M.G. 2008 Turbulence-condensate interaction in two dimensions. *Phys. Rev. Lett.* **101**, 194504.